



Synthesis, characterisation and electroluminescence behaviour of π -conjugated imidazole–isoquinoline derivatives



N. Nagarajan^a, Asit Prakash^b, G. Velmurugan^a, Nanda Shakti^b, Monica Katiyar^{b,**}, P. Venunalingam^{a,*}, R. Renganathan^{a,1,*}

^aSchool of Chemistry, Bharathidasan University, Tiruchirappalli 620 024, Tamil Nadu, India

^bDepartment of Materials Science & Engineering and Samtel Centre for Display Technologies, Indian Institute of Technology Kanpur, Kanpur 208016, India

ARTICLE INFO

Article history:

Received 6 September 2013
Received in revised form
31 October 2013
Accepted 3 November 2013
Available online 13 November 2013

Keywords:

Imidazole
Isoquinoline
Blue light
Pure white light
Electromer
TD-DFT

ABSTRACT

A series of highly fluorescent, isoquinoline π -conjugated imidazole derivatives have been synthesized and fully characterized. Their photophysical, electrochemical and thermal properties have also been discussed. The interplay of amorphous and crystalline nature of the compounds in thin film and fine powder have been analysed by using X-ray diffraction and atomic force microscopic (AFM) techniques. An organic light emitting diode consisting of 4-(4-(1-(4-methoxyphenyl)-4,5-diphenyl-1H-imidazol-2-yl)phenyl)isoquinoline as the emitting layer doped with 4,4'-Bis(N-carbazolyl)-1,1'-biphenyl (CPB) showed ideal blue emission (CIE: 0.16, 0.08). "Pure" white light (CIE: 0.34, 0.32) comprising of a blue light from excimers and an orange light from electromers at a high voltage has been achieved by using the compounds 2-(4-(isoquinolin-4-yl)phenyl)-1H-phenanthro[9,10-d]imidazole & 2-(4-(isoquinolin-4-yl)phenyl)-1-(4-methoxyphenyl)-1H-phenanthro[9,10-d]imidazole as single-emitting components. To elucidate the structural and optical properties, computational calculations have been performed. Computed results reveal all the electronic transitions are of $\pi \rightarrow \pi^*$ type and energy of the $S_0 \rightarrow S_1$ follows same variation trend with the band gap.

© 2013 Elsevier Ltd. All rights reserved.

1. Introduction

Since Tang and co-workers [1] report of an archetypical example of a modern Organic light emitting diodes (OLEDs), it has been a topic of great interest for many researchers due to their applications in lighting and flat panel displays. A wide variety of improvements to OLEDs have been made using novel materials and device structures to achieve improved efficiency at simple synthetic routes, easy device fabrication and low driving voltages [2–5]. The hunt for efficient blue and white electroluminescence is of particular interest because it is an essential component to realise OLEDs in display as well as lighting applications. Many research groups have successfully prepared efficient blue [6,7] and white fluorophores [8,9] for OLEDs, but efficient one, which can match the National Television System Committee (NSTC) and Commission Internationale d'Éclairage standard blue CIE (x,y) coordinates of (0.14, 0.08) and white (0.33, 0.33) has been achieved by very few

compounds. But most of them lack amorphous nature in thin films and OLEDs usually require formation of very thin organic layers with amorphous morphologies that provide pinhole free thin films.

Compared to the multi-emitting-component WOLEDs, a single-emitting-component WOLEDs could show many advantages, such as better stability, better reproducibility, and a simpler fabrication process. However, few materials are known to show white-light emission as a single-emitting component but synthesized by multistep process, among them very few have been reported to emit "pure" white light [10–12]. Therefore, the search for new organic light-emitting materials with new structures for use in single-emitting-component WOLEDs is of obvious interest and importance. Excluding the utilisation of mixture of three organic components emitting three colours (blue, green, and red) to get white light [13,14], a widely employed approach in recent years is the use of single chromophore that emits white light resulted from the combination of its monomeric (blue) and excimeric or electromeric (orange) emission [15–18]. The latter emission results from a stacking of molecules that is usually induced by π – π interactions.

Materials containing aromatic heterocyclic segments, e.g., quinoline [19,20], and oxidazole [21], had been reported to exhibit better electron injection and transport ability, but these materials

* Corresponding authors. Tel.: +91 431 2407053; fax: +91 431 2407045.

** Corresponding author.

E-mail address: rrengas@gmail.com (R. Renganathan).

¹ Tel.: +91 431 2407053; fax: +91 431 2407045.

were found to be undesirable as emitting layers in OLEDs due to their low luminance [22]. The typical heterocyclic molecule, imidazole with N1, C2, C4 and C5 positions substituted with different groups are used extensively in OLEDs for efficient blue [23–25] and white light applications [26]. Herein, we report the synthesis, crystal structure, film forming behaviour, photophysical, photo and electroluminescence properties of imidazole substituted isoquinoline derivatives. These new π -conjugated compounds, in particular, the phenanthrene based compounds, can serve as a single-emitting component for WOLEDs, emitting almost “pure” white light with stable CIE coordinates under different driving voltages.

2. Experimental section

2.1. General methods

The ^1H and ^{13}C NMR spectra were measured on a Bruker Avance 400 (400 MHz) NMR spectrometer. Mass spectra were obtained on an FDMS, VG Instruments ZAB-2 mass spectrometer. Steady state spectroscopic measurements were conducted both in solution and thin films prepared by vacuum (2×10^{-6} mbar) deposition on a quartz plate. The thickness of films was measured using Alpha Step profilometer (KLA Tencor). Absorption spectra of solution and thin film were obtained using UV–vis spectrophotometers (JASCO V360). Photoluminescence emission spectra of solution and thin film were obtained using fluorescence spectrophotometer (PerkinElmer – LS55 & Horiba Jobin Yvon FluoroLog 3 Spectrofluorometer). Photoluminescence quantum efficiencies (Φ_{PL} values) for solutions were obtained using 9,10–diphenylanthracene as reference [27]. The Φ_{PL} values of thin films on quartz plates were measured using a 6 inch integrating sphere (Labsphere) attached with Horiba Jobin Yvon FluoroLog 3 Spectrofluorometer through optical fibre and a PMT detector (Hamamatsu). Thermogravimetric analyses (TGA) and differential scanning calorimetry (DSC) were performed under nitrogen atmosphere at heating rate of $10^\circ\text{C}/\text{min}$. Melting points were determined by the open capillary tube method using a Toshniwal melting point apparatus and are uncorrected. The topography of the thin films was analysed by Atomic Force Microscopy imaging ($5 \times 5 \mu\text{m}$ and $2 \times 2 \mu\text{m}$) using acoustic AC mode with a silicon nitride tip (resonance frequency of 295 kHz), in order to evaluate the effect of thermal stress on the thin film morphology. Fluorescence lifetime measurements were carried out in a picosecond time correlated single photon counting (TCSPC) spectrometer. The excitation source is the tunable Ti–sapphire laser (Tsunami, Spectra Physics, USA). The fluorescence decay was analysed by using the software provided by IBH (DAS-6).

2.2. Syntheses

2.2.1. Synthesis of 4-(isoquinolin-4-yl)benzaldehyde (2)

4-bromoisquinoline (1) (1 g, 4.7 mmol) was treated with 4-formylphenylboronic acid (0.77 g, 5.17 mmol), $\text{Pd}[\text{PPh}_3]_4$ (0.27 g, 0.235 mmol), K_2CO_3 (1.94 g, 14.1 mmol) in THF (50 ml) at 70°C under nitrogen atmosphere for 12 h and progress of the reaction was monitored by TLC. The reaction mixture was quenched with water, extracted with CH_2Cl_2 and washed with brine ($2 \times 10 \text{ mL}$). The organic layer was separated, dried over anhydrous Na_2SO_4 and concentrated under reduced pressure. The crude product was purified by column chromatography (EtOAc/hexane) to afford pure 4-(isoquinolin-4-yl)benzaldehyde. The yields and important spectral data are given below.

^1H NMR (CDCl_3): 7.66 (4H, m), 7.83 (1H, d, 8.4 Hz), 8.02 (3H, m), 8.47 (1H, s), 9.26 (1H, s), 10.09 (1H, s); ^{13}C NMR: 53.5, 76.9, 77.3, 77.6, 124.1, 127.4, 128.0, 128.3, 129.3, 130.7, 131.0, 131.9, 133.5, 135.7, 142.7, 143.2, 152.7, 191.7.

2.2.2. Synthesis of compounds 1–4

A mixture of corresponding diketone (1 mmol), 4-(isoquinolin-4-yl)benzaldehyde (1 mmol), p-anisidine (4 mmol, in case of 2 & 4), ammonium acetate (4 mmol) and glacial acetic acid (8 mL) was refluxed for 4 h under nitrogen atmosphere. After cooling to room temperature, the reaction mixture was poured into distilled water with stirring. The separated solid was filtered off, washed with water and dried to give the expected product in good yields.

2.2.2.1. 4-(4-(4,5-diphenyl-1H-imidazol-2-yl)phenyl)isoquinoline (1). ^1H NMR ($\text{DMSO}-d_6$): 7.24 (1H, d, 7.2 Hz), 7.31 (2H, t, 7.6 Hz), 7.39 (1H, d, 7.2 Hz), 7.45 (2H, t, 7.6 Hz), 7.53 (2H, d, 7.2 Hz), 7.58 (2H, d, 7.6 Hz), 7.67 (2H, d, 8.4 Hz), 7.75 (1H, m), 7.82 (1H, m), 7.93 (1H, d, 8 Hz), 8.23 (1H, d, 7.6 Hz), 8.28 (2H, m), 8.52 (1H, s), 9.36 (1H, s), 12.84 (1H, s); ^{13}C NMR: 123.9, 125.4, 126.5, 127.1, 127.5, 127.7, 128.0, 128.1, 128.2, 128.4, 128.6, 129.9, 130.2, 130.9, 131.1, 131.3, 132.0, 133.0, 135.1, 136.0, 137.3, 142.4, 145.1, 152.0; HRMS (ESI) calcd for $\text{C}_{30}\text{H}_{21}\text{N}_3$ ($\text{M} + \text{H}$) $^+$ 424.1813, found 424.1816.

2.2.2.2. 4-(4-(1-(4-methoxyphenyl)-4,5-diphenyl-1H-imidazol-2-yl)phenyl)isoquinoline (2). ^1H NMR (CDCl_3): 3.79 (3H, s), 6.85 (2H, d, 8.8 Hz), 7.07 (2H, d, 8.8 Hz), 7.19 (3H, m), 7.25 (6H, m), 7.42 (2H, d, 7.2 Hz), 7.63 (5H, m), 7.91 (1H, d, 8 Hz), 8.01 (1H, d, 7.6 Hz), 8.46 (1H, s), 9.24 (1H, s); ^{13}C NMR: 55.4, 114.3, 124.7, 126.6, 127.2, 127.3, 127.9, 128.0, 128.2, 128.4, 128.6, 128.9, 129.5, 129.8, 129.9, 130.4, 130.6, 130.7, 131.1, 131.4, 132.7, 134.0, 134.5, 136.7, 138.4, 142.8, 146.5, 152.1, 159.3; HRMS (ESI) calcd for $\text{C}_{37}\text{H}_{27}\text{N}_3\text{O}$ ($\text{M} + \text{H}$) $^+$ 530.2232, found 530.2235.

2.2.2.3. 2-(4-(isoquinolin-4-yl)phenyl)-1H-phenanthro[9,10-d]imidazole (3). ^1H NMR ($\text{DMSO}-d_6$): 7.65 (2H, m), 7.81 (6H, m), 7.98 (1H, d, 8.8 Hz), 8.26 (1H, d, 8 Hz), 8.51 (2H, d, 8.4 Hz), 8.57 (2H, m), 8.63 (1H, d, 7.2 Hz), 8.87 (2H, m), 9.39 (1H, s), 13.60 (1H, s); ^{13}C NMR: 121.9, 123.9, 1254.3, 126.4, 127.1, 127.5, 128.0, 128.1, 129.9, 130.4, 131.2, 131.9, 133.0, 137.1, 142.4, 148.7, 152.2; HRMS (ESI) calcd for $\text{C}_{30}\text{H}_{19}\text{N}_3$ ($\text{M} + \text{H}$) $^+$ 422.1657, found 422.1655.

2.2.2.4. 2-(4-(isoquinolin-4-yl)phenyl)-1-(4-methoxyphenyl)-1H-phenanthro[9,10-d]imidazole (4). ^1H NMR (CDCl_3): 3.96 (3H, s), 7.14 (2H, d, 8.8 Hz), 7.27 (2H, m), 7.46 (5H, m), 7.65 (3H, m), 7.68 (1H, m), 7.78 (2H, m), 7.90 (1H, d, 8.4 Hz), 8.04 (1H, d, 7.6 Hz), 8.47 (1H, s), 8.71 (1H, d, 8.0 Hz), 8.78 (1H, d, 8.4 Hz), 8.90 (1H, d, 8.0 Hz), 9.25 (1H, s); ^{13}C NMR: 55.7, 115.3, 120.9, 122.7, 123.1, 124.1, 124.6, 124.9, 125.6, 126.3, 127.2, 127.9, 128.3, 128.4, 128.5, 129.3, 129.4, 130.0, 130.1, 130.3, 130.7, 131.2, 132.7, 134.0, 137.4, 142.6, 150.6, 152.1, 160.4; HRMS (ESI) calcd for $\text{C}_{37}\text{H}_{25}\text{N}_3\text{O}$ ($\text{M} + \text{H}$) $^+$ 528.2075, found 528.2074.

2.3. Computational details

All calculations on the synthesized molecules have been performed using Gaussian 09 [28]. The ground-state geometries of the studied molecules were fully optimized at the DFT level using B3LYP [29–32] functional with 6-31G(d,p) basis set and the excited state geometries were optimized by the ab initio configuration interaction singles method (CIS) [33]. The vibrational frequency analysis of the optimized geometries confirms that all the optimized geometries are found to be of minimum energy on the potential energy surface by exhibiting all real frequencies. The electronic absorption and emission spectra, both in vacuum and in solvent, were systematically investigated by the time-dependent density functional theory (TD-DFT) [34–37] method at PBE0 [38–39]/6-31+G(d,p) level. The solvent

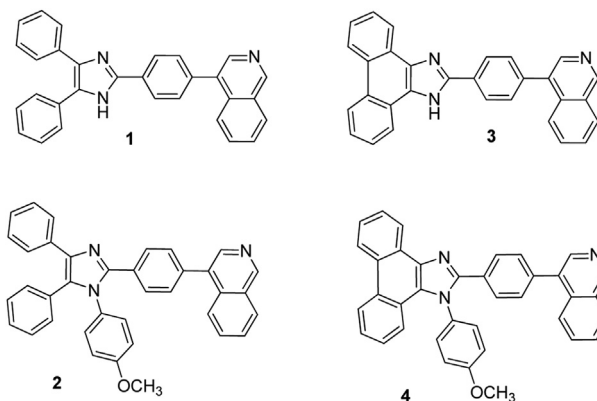
effect has been included by the polarized continuum model (PCM) [40].

2.4. OLED fabrication

Prior to device fabrication, ITO on glass was patterned as 6 mm wide stripes with a resistivity of $15\text{--}20 \Omega \text{ cm}^{-2}$ and then pixelized using photolithography technique of $4 \text{ mm} \times 4 \text{ mm}$ to reduce the leakage current. The substrates were cleaned by sonication in soap solution, rinsed with deionized water, acetone and isopropyl alcohol for 10 min in each solvent and dried with nitrogen. Finally, the substrates were treated with UV ozone for 10 min. The aqueous solution of PEDOT:PSS [poly(3,4-ethylenedioxythiophene) poly(styrenesulfonate)] was spin coated at 1500 rpm for 1 min to form a 40 nm hole injecting layer (HIL). Organic layers were deposited sequentially by thermal evaporation from resistively heated tungsten boats and crucible onto the substrate at a rate of 1 \AA s^{-1} . The base pressure at room temperature was $3\text{--}4 \times 10^{-6}$ mbar. The deposition rate and the thickness were measured with a quartz control monitor located near the substrate holder. After organic film deposition, the substrate was transferred to glove box and the chamber was vented to load the cathode sample. A cathode consisting of 0.5 nm LiF or 16 nm calcium followed by aluminium was deposited at a rate of 0.1 \AA s^{-1} for LiF, 0.3 \AA s^{-1} for calcium and 2 \AA s^{-1} for aluminium. The devices were tested in air within 10 h of fabrication. Only light emitting from the front face of the OLEDs was collected and used in subsequent efficiency calculations. The optical properties of fabricated devices such as current–voltage–luminance ($I\text{--}V\text{--}L$) characteristics, electroluminescence spectra (EL) and CIE colour coordinates have been done using CS-1000 spectro-radiometer (Konica Minolta) and Keithley 2400 source metre interfaced with computer under dark room.

2.5. Crystallographic measurements

Crystals of 2 and 4 were grown from $\text{CH}_2\text{Cl}_2/\text{n-hexane}$ at room temperature. The preliminary examination and data collection were performed using a Bruker kappa Apex II CCD detector system single-crystal X-ray diffractometer equipped with a fine-focus sealed X-ray tube using graphite-monochromated $\text{Mo K}\alpha$ radiation ($\lambda = 0.71073 \text{ \AA}$). Structure solution and refinement were carried out using the X Shell and SHELXL-97 software package. The unit-cell parameters were obtained by least-squares fit to the automatically centred settings for reflections. All calculations were performed using the WINGX software package and SHELX programme. Structure solution was done by direct method and refined by a full-matrix least-squares method on F^2 (F : structure factor).



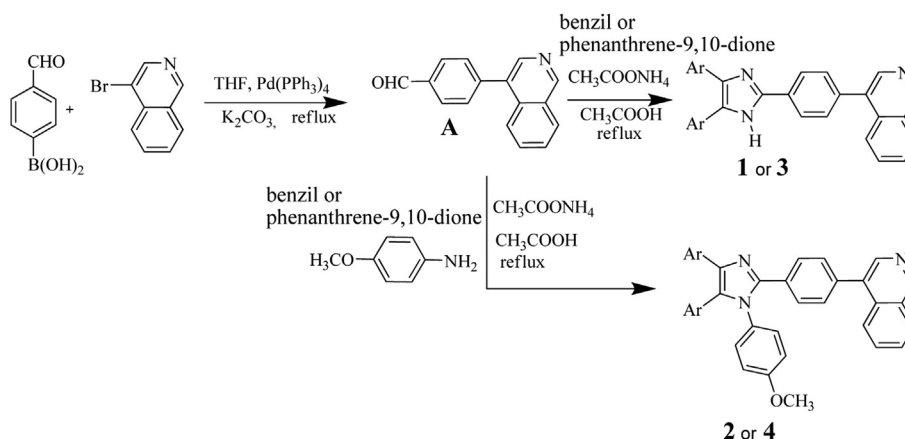
Scheme 1. Structures of the synthesized compounds.

3. Results and discussion

The chemical structure of the synthesized compounds (Scheme 1) and synthetic route are shown in Scheme 2. 4-bromoisoquinoline and 4-formylphenyl boronic acid were commercially obtained and compound A can be easily prepared by using one step Suzuki coupling reaction and it was isolated and purified by column chromatography on silica gel with good yields (85%) and high purity. The compound A was then involved in multicomponent cyclization with respective diketone and amine in presence of ammonium acetate and acetic acid to give the target emitters 1–4. The molecular structure of the synthesized compounds were confirmed with NMR, Mass spectrometry and single crystal X-ray diffraction (for compound 2 & 4) analysis.

3.1. X-ray crystallography

Single crystal X-ray diffraction studies were used to further confirm the structure of 2 (Fig. S1) and 4 (Fig. S2). Crystals 2 and 4 crystallized in a triclinic and monoclinic crystal system in P21/n and P-1 space group respectively. The important bond lengths, bond angles and dihedral angles are listed in Table S1 and structural refinement data are listed in Table S2. The twist angle between the imidazole ring and 4-methoxy phenyl ring for 2 and 4 are $90.3(5)$ and $72.9(2)$ respectively. The free rotation of phenyl groups attached in C4 and C5 position in 2 leads to high twist angles about $83.4(5)$ and $24.2(5)$ but which is restricted in 4 leads to planar structure of phenanthrene moiety. The restricted free rotation also



Scheme 2. Synthetic pathway used for the preparation of compounds 1–4.

Table 1
Optical, electrochemical and thermal properties of the compounds.

	λ_{abs} (nm) ^a soln	λ_{em} (nm) ^a soln	λ_{abs} (nm) film	λ_{em} (nm) film	$\epsilon \times 10^3$ (M ⁻¹ cm ⁻¹)	$T_g/T_m/T_d5$ (°C)	$E_{\text{Onset}}^{\text{ox}}$ (V)	E_g^b (eV)	HOMO/LUMO ^c (eV)
1	333	442	334	443	35.5	112/254/338	1.14	3.18	-5.49/-2.31
2	328	432	329	421	28.5	102/220/334	1.32	3.12	-5.67/-2.55
3	370	435	355	448, 494	12.8	167/280/362	1.24	3.24	-5.59/-2.35
4	365	429	349	450	32.3	108/252/343	1.33	3.17	-5.68/-2.57

^a Absorption and emission spectra were measured in THF solution ($<10^{-5}$ M) $\lambda_{\text{em}} = \lambda_{\text{exc}}$.

^b Estimated from onset of the absorption spectra $E_g = (1240/\lambda_{\text{onset}})$.

^c The HOMO and LUMO energies were determined from cyclic voltammetry and the absorption onset. Ferrocene (4.8 eV) was used as the internal standard in each experiment. The ferrocene oxidation potential was located at +450 mV, relative to the Ag/AgNO₃ non-aqueous reference electrode.

reduces the twist angle between the imidazole ring and 4-methoxy phenyl ring in 4. Further details regarding the crystal structure can be found from the CCDC 917839 for 2 and CCDC 917481 for 4.

3.2. Optical properties

Photophysical properties of the four compounds were investigated by measuring the PL spectra in both THF solutions as well as solid-state thin films on quartz substrates. Key data are summarized in Table 1. As can be seen in Fig. 1, all compounds exhibit broad structureless emission peaks ranging from 418 to 487 nm. It should be noted that the compounds 1 and 2 show negligibly small peak shifts in their absorption and PL spectra from THF solutions to solid states. This indicates that the highly twisted substituent on the 1H-imidazole position as well as the non-coplanar phenyl moiety at C4 and C5 position can effectively suppress the intermolecular π - π stacking in the solid state. On the other hand, it is worth noting that the absorption and PL spectrum of 3 and 4 is broadened and more red-shifted in solid thin films. The observed high FWHM of 138 nm and 104 nm for 3 and 4 may be attributed to the intermolecular π - π stacking in the solid state. It can be evidenced from the crystal packing arrangement of 4, in which we noticed strong edge-to-face π - π interaction between the C22 & C23 carbon of the phenyl group attached to the isoquinoline moiety with one of the centre core ring of phenanthrene moiety. The distance between these π - π stacking interaction is around 3.5–3.8 Å which are shown in Fig. S3. Thus, the molecular architecture in which conjugated units is stacked to one another in such a way that strong electronic interactions can occur over the entire moiety. Notably, 3 shows more bathochromic shift and two distinct peaks viz., a shoulder at 448 nm may be ascribed to the normal emission and major emission at 494 nm may be ascribed to the influence of stacking interaction in solid state [41,42]. This observed effect is more prominent in 3 and not in 4 possibly due to the absence of 4-methoxy phenyl moiety at 1H-

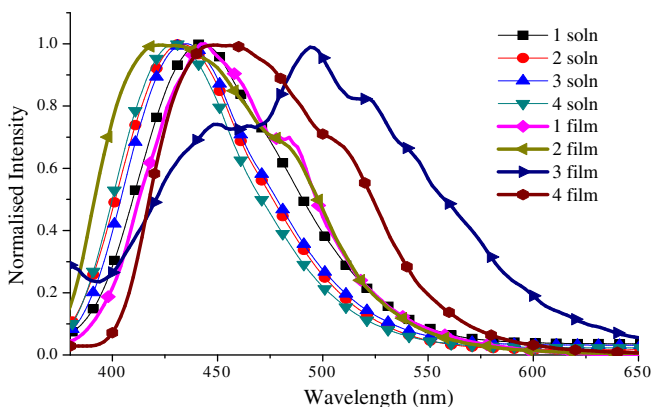


Fig. 1. Photoluminescence spectra of compounds in THF solution (thin line) and thin films (thick line).

position of imidazole group, which can further increase the π - π interaction in 3.

From the absorption spectra (Fig. S4), it can be seen that all the compounds show similar absorption bands at a shorter wavelength of approximately 270 nm, which can be attributed to the π - π^* transition of their common benzene ring and the longer wavelength absorption bands in the range of 325–374 nm, which can originate from the π - π^* transition of the substituent's on the C2-position of the imidazole ring. The fluorescence quantum yields (Φ_f) were measured sequentially in solution as well as in solid films to be as high as 0.54 to 0.93 for solutions and 0.27 to 0.69 for solid films (Table 2). From Fig. S5, the fluorescence decay profiles of all the compounds in THF ($\tau_f \approx 0.99$ –1.12 ns) could be satisfactorily fitted well in monoexponential decay with a χ^2 values of nearly unity, indicating that the emission from a single excited state in each case. Thus, the possibility of the imidazole and isoquinoline moieties behaving as two separate chromophoric units can be ruled out. The calculated radiative (k_r) and nonradiative (k_{nr}) decay constants (Table 2) suggest that the energy of electronically excited state is mainly dissipated by radiative transition pathway. With these overall photophysical properties of the compounds, we suggested that these compounds can be utilised as better candidates for OLED applications.

3.3. Thermal properties

Thermogravimetric analysis (TGA) and differential scanning calorimetry (DSC) were employed to investigate the thermal properties of the compounds; the related data are listed in Table 1. As shown in Fig. S6(A), decomposition temperatures (T_d), defined as the temperature at which the materials show a 5% weight loss, were measured to be 338, 334, 362 and 343 °C for 1–4 respectively. From the DSC measurement (Fig. S6(B)), it is important to note that all the compounds have high glass transition temperature (T_g) of 112 °C, 102 °C, 167 °C and 108 °C for 1–4 respectively. Such high T_g values imply that they could form morphologically stable amorphous films upon thermal evaporation, which is highly important for application in OLEDs.

3.4. Electrochemical properties

To probe the electrochemical properties of the new compounds, cyclic voltammetry (CV) measurements have been performed in a

Table 2
Quantum yield (Φ_f) in both thin film and solution, lifetime (τ_f), radiative (k_r) and nonradiative (k_{nr}) decay constant values of the compounds.

	Φ_f^a film	Φ_f^b soln	τ_f (ns)	k_r (10^8 s ⁻¹)	k_{nr} (10^8 s ⁻¹)
1	0.46	0.60	0.99	6.07	4.03
2	0.64	0.76	1.06	7.17	2.25
3	0.27	0.54	1.12	4.85	4.07
4	0.69	0.93	1.10	8.41	0.61

^a Calculated by using integrating sphere method.

^b Calculated by using 9, 10-diphenylanthracene as a reference in ethanol ($\Phi_f = 0.95$) solution ($<10^{-5}$ M).

three-electrode cell setup with 0.1 M tetrabutylammonium hexafluorophosphate (TBAPF6) as the supporting electrolyte and ferrocene (Fc) as the internal standard. Representative cyclic voltammograms are shown in Fig. S7. The details of the electrochemical properties of these compounds are listed in Table 1. During anodic scans between 0 and 2 V in DMF, only one oxidation peak is observed at 1.34, 1.45, 1.49 and 1.55 V for 1, 2, 3 and 4 respectively. A one-electron irreversible oxidation wave observed for all compounds is attributed to the oxidation of the imidazole based conjugated spacer and electron-rich methoxy segments which increase the oxidation ability of the compounds (2 and 4) and they show more anodically shifted redox potentials. This is consistent with results reported in the literature for the electrochemical behaviour of imidazole and its derivatives [43,44]. The energy levels of the HOMOs of these materials were calculated with reference to ferrocene (4.8 eV) and the values ranges from –5.4 to –5.7 eV. These together with absorption spectra were then used to obtain the LUMO energy levels (Table 1).

3.5. Morphology

Furthermore, to investigate the morphology of the films, thin film of the compounds have been prepared on quartz plate substrates by vacuum deposition and imaged by atomic force microscopy (AFM). In order to evaluate the stability of the thin films, the surface has been exposed to air under thermal stress conditions from room temperature to 100 °C. The non-heated film surface presents a regular and smooth morphology (Fig. S8(a) and (b)) and surface roughness (Ra) of the film appears to be very low, around 1–3 nm. Interestingly, the roughness is kept almost unchanged of annealing at 100 °C which is highlighting the very good quality of the film surface (Fig. S8(c) and (d)) and the high stability of the compounds upon exposure to stress circumstances. In addition, the powder X-ray diffraction (XRD) measurement has been carried out to envisage the nature of thin films. As shown in Fig. S9(A), the thin films of 1 and 2 both show relatively broad and random scattering peaks clearly demonstrating the non-crystalline amorphous nature of compounds. In contrast, the powder form of the compounds 1 and 2 shows notable sharp peaks (Fig. S9(B)) in XRD measurement implies that the compounds have crystalline nature in powder state which turns into the amorphous nature on thin films. In this context, amorphous films are most appropriate for practical applications, since in crystalline films the existence of number of inter-crystalline boundaries that limit the charge mobility and give rise to morphological inhomogeneities [45]. The excellent morphological stability under very harsh conditions and non-crystalline amorphous nature of films is a key point for any possible OLED applications [46].

3.6. OLED device performance

To investigate the EL properties of the compounds 1–4 as an emitting layer (EML), a series of devices (I–V) with different device configuration have been fabricated and the results are shown in Table 3. Initially, simple devices consisting of [ITO/PEDOT:PSS(40 nm)/NPB (30 nm)/EML (40 nm)/LiF (0.5 nm) or Ca (16 nm)/Al(100 nm)] have been fabricated. Where PEDOT:PSS was the hole injecting layer (HIL), NPB [N,N'-Di(naphthalen-1-yl)-N,N'-diphenyl-benzidine] was employed as the hole-transporting layer (HTL) and LiF/Al or Ca/Al was employed as the cathode. From these device configurations, we observed poor device performance for 1 and 2. This can be ascribed to the unfavourable alignment of energy levels of different layers to recombine the generated exciton within the emissive layer (Fig. S10). Hence, we modified the device configuration by introducing BCP [2,9-Dimethyl-4,7-diphenyl-1,10-

Table 3

Electroluminescence performance of devices I–V for the compounds 1–4.

Device	Emitters	EL (nm)	V_{on}^a (V)	L^b (Cd m ⁻²)	η_c^c (Cd A ⁻¹)	CIE (x,y)
I	1	612	8.5	<1	–	0.46, 0.37
II	1	600	12.5	<1	–	0.44, 0.41
III	1	497	8.5 V	221	0.99	0.29, 0.42
I	2	473	12	5	–	0.24, 0.29
III	2	450	8.5 V	37.5	0.20	0.20, 0.20
IV	2	438	5.5	591	–	0.16, 0.08
III	3	452, 600	15 V	7.9	0.19	0.34, 0.32
III	4	499, 614	17	<1	–	0.36, 0.35
V	4	512, 650	21	<1	–	0.37, 0.37

Device I: ITO/PEDOT:PSS(40 nm)/NPB (30 nm)/EML (40 nm)/LiF (0.5 nm)/Al (100 nm).

Device II: ITO/PEDOT:PSS(40 nm)/NPB (30 nm)/EML (40 nm)/Ca (16 nm)/Al (100 nm).

Device III: ITO/NPB (60 nm)/EML (40 nm)/BCP (15 nm)/Alq₃ (20 nm)/LiF (0.5 nm)/Al(100 nm).

Device IV: ITO/NPB (60 nm)/CBP: 10% EML (40 nm)/TPBi (20 nm)/LiF (0.5 nm)/Al (100 nm).

Device V: ITO/EML (130 nm)/LiF (0.5 nm)/Al (100 nm).

^a V_{on} : turn-on voltage.

^b L : Luminance.

^c η_c : current efficiency.

phenanthroline] as the hole blocking layer (HBL) and Alq₃ as the electron transporting layer (ETL). The fabricated device configuration is [ITO/NPB (60 nm)/EML (40 nm)/BCP (15 nm)/Alq₃ (20 nm)/LiF (0.5 nm)/Al(100 nm)]. Herein, the enhanced device performance has been registered for 1 and 2 compared with previous one (Table 3). The combined PL and EL spectra of 1 and 2 in different device configuration (II, III and IV) are shown in Fig. 2.

For 1, the red shifted EL spectrum at 497 nm with maximum luminance of 221 Cd m⁻² (CIE: 0.29, 0.42) with turn on voltage of 8.5 V and maximum efficiency of 0.99 Cd A⁻¹ has been achieved. The observed EL spectrum and CIE coordinates correspond with yellowish green colour. In turn, compound 2 shows the EL spectrum at 450 nm with turn on voltage of 8.5 V and maximum luminance of 37.5 Cd m⁻² (CIE: 0.20, 0.20). As this device has the EL behaviour related to blue colour, we further modified the device configuration to achieve our primary interest of getting pure colour. For that, we doped the compound 2 with CPB [4,4'-Bis(N-carbazolyl)-1,1'-biphenyl] because CPB can act as a host as well as hole transporting layer which can help for efficient exciton recombination in the emissive layer. The device configuration is [ITO/NPB (60 nm)/CBP: 10% EML (40 nm)/TPBi (20 nm)/LiF (0.5 nm)/Al(100 nm)], where TPBi [1,3,5-Tri(1-phenyl-1H-benzo[d]imidazol-2-yl)phenyl] was employed as the hole blocking layer and electron transport layer.

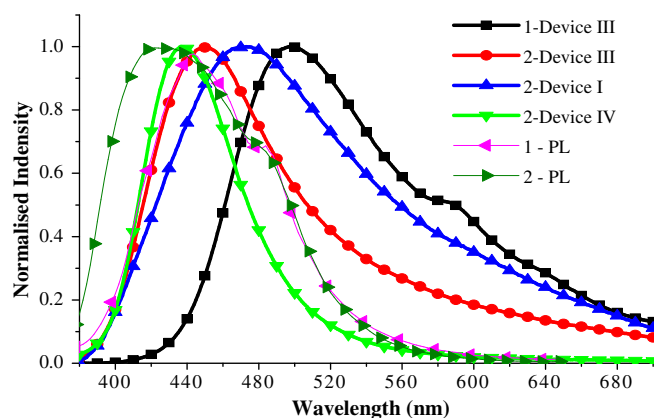


Fig. 2. PL (thin line) and EL (thick line) spectra of 1 and 2 in various device configurations.

From this device, we observed better device performance with brightness of 591 Cd m^{-2} at 18 V and turn on voltage of 5.5 V and achieved almost pure blue light (CIE: 0.16, 0.08) and EL spectrum at 438 nm. The observed CIE coordinates are well matched with the standard values suggested by NSTC and CIE for pure blue light (0.14, 0.08). It implies that the exciton recombination is well confined within the CBP molecular layer which is hosting emitter 2.

Interestingly, the emitters 3 and 4 in device III configuration exhibited white EL with the spectra covering the whole visible range as a result of the combination of the blue and orange emission. Devices based on 3 and 4 showed pure white light with CIE coordinates of 0.34, 0.32 (Fig. 3) and 0.36, 0.35 at 17 V (Fig. 4), with the brightness values of 8 and 0.25 Cd m^{-2} respectively. Even though these preliminary results are inferior to those of recently reported white OLEDs, efficient single-emitting component white OLEDs are expected after optimizing the device configuration.

The EL spectra of the devices differ significantly from their PL spectra. The emission in the blue region resembles with the respective PL of each compound and it evidently originates from the singlet-excited state of an individual molecule. The emission in the orange region with a peak at about 620–650 nm for 3 and 4 does not appear in the PL spectrum either in the solution or in the film, indicating that the orange emission is a peculiar characteristic of the EL. This interesting feature normally observed due to the aggregates or electromer or electroplex. To check the possibility of electroplex formation [excited state complex formed between two different compounds in the device configuration (X^+/Y^-)*] in the EL spectrum, the single layer devices with 130 nm of compound 4 sandwiched between ITO and LiF/Al electrodes are fabricated. The EL spectra of the single layer device are shown in Fig. 4.

Obviously, the emissive features of the single layer device are quite similar to the EL spectra of multilayer one. This result indicates that the orange emission is an inherent property for the EL of the molecules and the electroplex emission as the source of the long wavelength emission band is cast away. It is thus plausible to assign the additional orange emission band to electromer produced only by electric excitation. We infer that the orange emission in our single layer and multilayer devices can arise from the electromer ($3^+/3^-$)* and ($4^+/4^-$)*. The energy of such a hole–electron pair trapped by two molecules would be lower than that of the monomer exciton. As a result, direct cross recombination of the electron and hole could result in emission at longer wavelengths compared to the PL of 3 and 4. It is hypothesised that the plausible driving force for the formation of electromer on electric excitation is the edge to face π – π interaction which would be expected to enhance

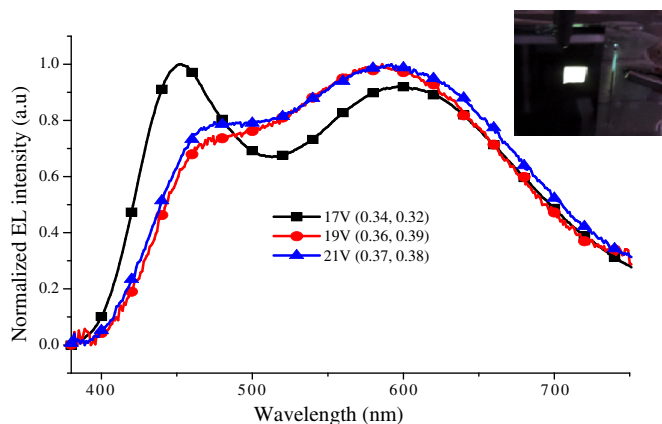


Fig. 3. EL spectra of compound 3 for device III in various applied voltages. Inset is photograph of device III for compound 3 at a driving voltage of 17 V.

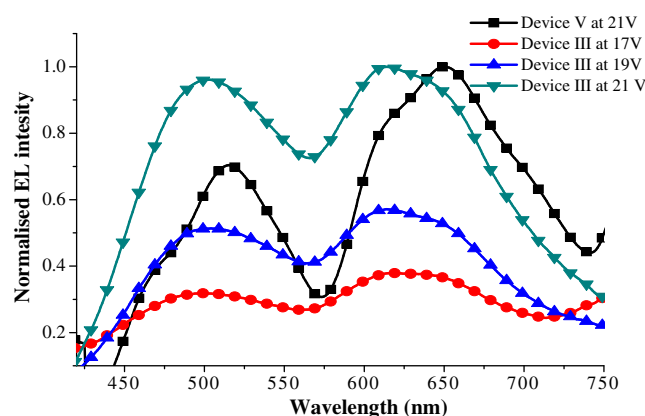


Fig. 4. EL characteristics of 4 in device III and V.

the electronic interaction within the molecules which can facilitate the formation of trapped level of hole–electron pair.

3.7. Geometry optimization and Frontier molecular orbitals

The optimized geometries of these compounds are depicted in Fig. S11. The selected important geometric parameters (bond lengths, bond angles and dihedral angles) of these compounds are in accordance with the X-ray data which is listed in Table S1. It will be useful to examine the highest occupied molecular orbitals (HOMOs), lowest unoccupied molecular orbitals (LUMOs) and band gaps (HOMO–LUMO gap) of the synthesized compounds since the relative ordering of the molecular orbitals provides qualitative indication of the excitation properties.

Therefore HOMOs and LUMOs of compounds 1–4 are investigated here, the plots of frontier molecular orbitals (from HOMO–3 to LUMO+3) and the corresponding energy level diagram are shown in Fig. 5. As observed in Fig. 6, it is interesting to note that the electronic cloud distribution of 1–4 of HOMO orbitals is spread over the imidazole core where as the LUMO is mainly centralized on the isoquinoline and phenyl part. Actually, the first dipole-allowed transitions correspond exclusively to the promotion of an electron from the HOMO \rightarrow LUMO as described in the absorption and emission section. From Fig. 5, it can be seen that the energy gaps of compounds 1–4 were found to be 3.66, 3.73, 3.63 and 3.65 eV respectively, which matches well with the electrochemically determined HOMO and LUMO potentials. From Fig. 5 and Table 4, it can be seen that, the calculated HOMO and LUMO energies and the excited energies (E_g) have the same variation with

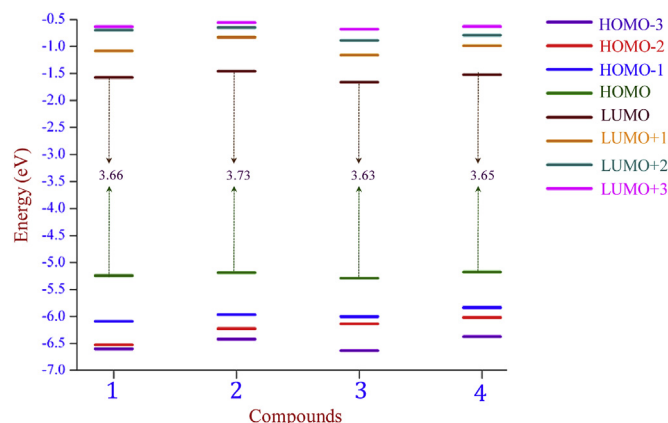


Fig. 5. Frontier molecular orbital levels of compounds 1–4.

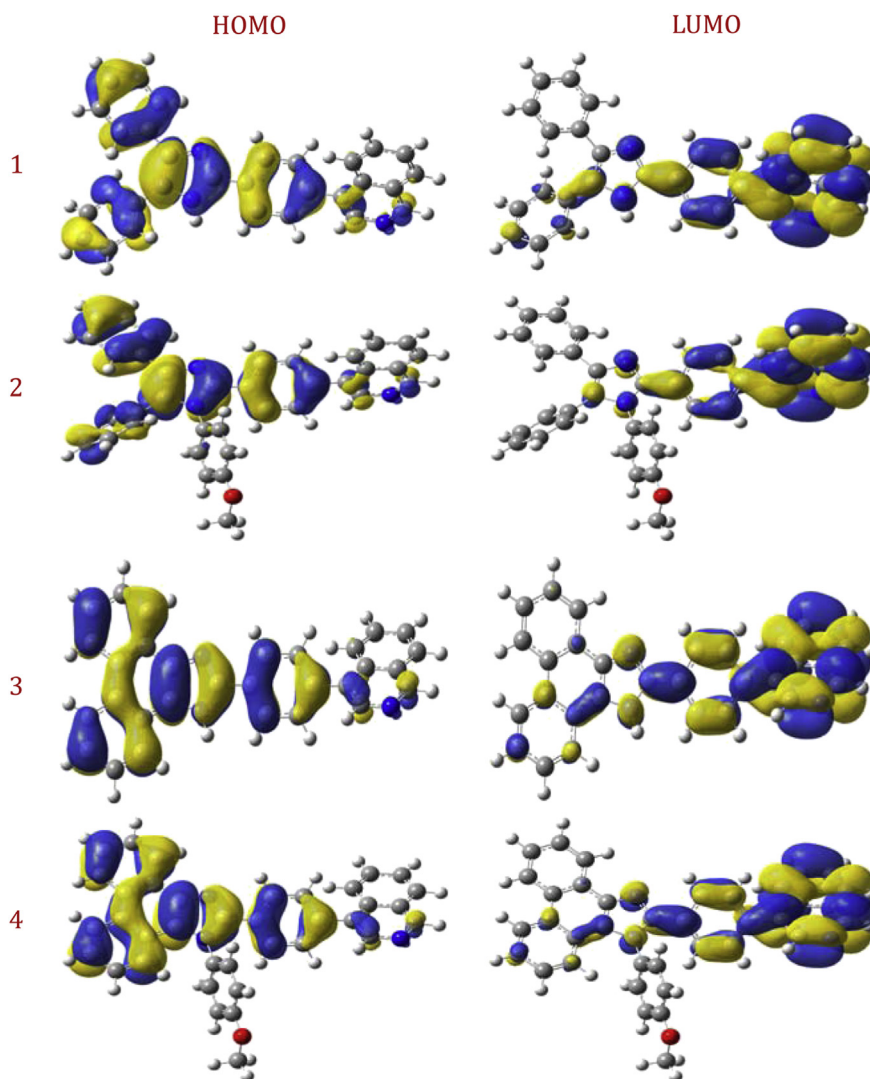


Fig. 6. Plots of HOMO and LUMO of 1–4 by DFT//B3LYP/6-31G(d,p).

the experimental data. The value of HOMO levels of 1–4 are -5.24 , -5.19 , -5.29 and 5.18 eV respectively and the LUMO levels are found to be -1.58 , -1.45 , -1.66 and -1.52 eV respectively.

It is essential to identify and understand the nature of various segments of the molecule and their individual contributions towards HOMOs and LUMOs for synthesizing newer molecules. Hence the contributions of various fragments of the molecules have been computed using QMForge [47] program. The whole molecule

has been segmented into two fragments, namely imidazole and isoquinoline part, their corresponding percentage contributions are summarized in Table S3. As evident from the molecular orbital diagrams, in all the compounds the contribution of the imidazole part is about 82% towards the HOMO level and interestingly LUMO is majorly stabilized by isoquinoline part with 90%. This indicates that these parts in 1–4 are responsible for the $\pi \rightarrow \pi^*$ transition upon excitation.

3.8. Computed absorption and emission spectra

To understand electronic transitions of these compounds, TD-DFT calculations on the absorption and emission spectra in both vacuum and solvent (THF) were performed. The lowest excited states were calculated by means of TD-DFT method and the effort to rationalize the nature of electronic transitions, the contributing configurations to the transitions and charge transfer probability. The calculated wavelengths from absorption and emission spectra, excitation energies, main transition configurations and oscillator strengths for the most relevant singlet excited states of each compound are summarized in Tables 4 and 5 respectively.

As shown in Table 4, all the electronic transitions are of the $\pi \rightarrow \pi^*$ type, and excitation to S_1 state corresponds to almost

Table 4

Computed absorption data obtained by TD-DFT (λ_{\max}) for compounds 1–4 at the B3LYP/6-31G(d,p) optimized geometry.

States	Electron transition	Expt λ_{\max} (nm)	Cal. λ_{\max} (nm)	Oscillator strength f	E (eV)	Major contribution
1 Gas-phase	$S_0 \rightarrow S_1$		362.3	0.6384	3.42	HOMO \rightarrow LUMO (96%)
THF	$S_0 \rightarrow S_1$	333	364.7	0.7950	3.40	HOMO \rightarrow LUMO (94%)
2 Gas-phase	$S_0 \rightarrow S_1$		354.3	0.4350	3.50	HOMO \rightarrow LUMO (95%)
THF	$S_0 \rightarrow S_1$	328	353.5	0.6019	3.51	HOMO \rightarrow LUMO (93%)
3 Gas-phase	$S_0 \rightarrow S_1$		366.4	0.8041	3.38	HOMO \rightarrow LUMO (95%)
THF	$S_0 \rightarrow S_1$	370	368.2	1.0268	3.37	HOMO \rightarrow LUMO (93%)
4 Gas-phase	$S_0 \rightarrow S_1$		362.7	0.6067	3.42	HOMO \rightarrow LUMO (94%)
THF	$S_0 \rightarrow S_1$	365	361.4	0.8553	3.43	HOMO \rightarrow LUMO (91%)

Table 5
Computed emission data obtained by TD-DFT for compounds 1–4 at the CIS/6-31G(d) geometry.

States	Electron transition	Expt λ_{\max} (nm)	Cal. λ_{\max} (nm)	Oscillator strength f	E (eV)	Major contribution
1 Gas-phase	$S_1 \rightarrow S_0$		408.2	0.8511	3.04	HOMO \rightarrow LUMO(99%)
THF	$S_1 \rightarrow S_0$	442	416.4	0.9865	2.98	HOMO \rightarrow LUMO(98%)
2 Gas-phase	$S_1 \rightarrow S_0$		415.4	0.9453	2.98	HOMO \rightarrow LUMO(99%)
THF	$S_1 \rightarrow S_0$	432	424.9	1.1314	2.92	HOMO \rightarrow LUMO(98%)
3 Gas-phase	$S_1 \rightarrow S_0$		411.5	1.2074	3.01	HOMO \rightarrow LUMO(99%)
THF	$S_1 \rightarrow S_0$	435	420.8	1.4229	2.95	HOMO \rightarrow LUMO(98%)
4 Gas-phase	$S_1 \rightarrow S_0$		413.6	1.1182	3.00	HOMO \rightarrow LUMO(99%)
THF	$S_1 \rightarrow S_0$	429	421.9	1.3648	2.94	HOMO \rightarrow LUMO(98%)

exclusively to the promotion of an electron from HOMO \rightarrow LUMO. The oscillator strengths (f) of the lowest $S_0 \rightarrow S_1$ electronic transition are the largest in these compounds. The excitation energies calculated for compounds 1–4 are 3.40, 3.52, 3.37 and 3.48 eV, respectively, which corresponds to the absorption wavelength of 364.7, 353.5, 368.2 and 361.4 nm, respectively. For the emission spectra, the emission peaks in THF solvent, with the largest oscillator strength for the compounds 1–4 are all assigned to $\pi \rightarrow \pi^*$ character, arising from the S_1 , HOMO \rightarrow LUMO transition (99%). The calculated values of the fluorescence wavelength in THF for 1–4 are located at 416.4, 424.9, 420.8 and 421.9 nm respectively. The calculated absorption and emission bands are in good agreement with the experimental results. The highest oscillator strengths of the $S_1 \rightarrow S_0$ transition for 1–4 imply that they have large fluorescent intensity and that they are useful as fluorescent OLED materials. Overall, the DFT and TD-DFT calculations reveal deeper insights into the electronic structures, optical properties and the nature of transition of the synthesized molecules.

3.9. Ionization potential, electron affinity and reorganization energy

The charge-injection/transport and their balance are crucial for optoelectronic compounds; therefore, it is important to investigate their ionization potentials (IPs), electronic affinities (EAs) and reorganization energies (λ) to evaluate the energy barrier for injection and transport rates of the holes and electrons. We calculated IPs and EAs, together with the hole extraction potential (HEP), which is the energy difference from M^+ (cationic) to M (neutral molecule) using the M^+ geometric structure, and the electron extraction potential (EEP), which is the energy difference from M^- (anionic) to M using the M^- geometric structure. The IPs and EAs can be either for vertical excitations (v , at the geometry of the neutral molecule) or adiabatic excitations (a , at the optimized structures for both the neutral and charged molecule).

The calculated reorganization energies are listed in Table S4. To be an emitting layer material, it needs to achieve the balance between hole injection and electron acceptance. By theoretical concept, if λ value is lower, the charge-transport rate will be higher. From Table S4, the λ_{hole} for 1–4 are lower than their respective $\lambda_{\text{electron}}$, suggesting that the hole transfer rate is higher than the electron transport rate. Hence, these compounds can be used as an HTL than the ETL. However, the energy differences between the λ_{hole} and $\lambda_{\text{electron}}$ is very small about 0.10, 0.04, 0.13, and 0.10 eV for the compounds 1–4 respectively, thus these compounds can also act as ambipolar material.

4. Conclusion

In summary, a series of substituted imidazole coupled with isoquinoline derivatives were synthesized by simple two step

processes and fully characterized. These compounds exhibited good thermal and morphological stabilities over very harsh conditions. Blue emission in solution and slightly red shifted emission in thin films with high PL quantum yields (0.27–0.93) were observed for these compounds. To elucidate the structural and optical properties of these compounds the DFT and TD-DFT calculations have been performed. A close agreement was found between the band gaps determined electrochemically (E_g) and those determined from the computational methods. The electronic transitions are of the $\pi \rightarrow \pi^*$ type, and excitation to S_1 state corresponds to almost exclusively to the promotion of an electron from HOMO \rightarrow LUMO in all the compounds. Accordingly, the energy of the $S_0 \rightarrow S_1$ electronic transition follows the same variation trend with the HOMO–LUMO energy gap of the molecule. The TD-DFT calculations lead to a good accordance with experimental absorption and emission spectra. Molecular structure dependant electroluminescence behaviour of the compounds was noticed in different device configurations. Compound 2 showed ideal blue colour (CIE: 0.16, 0.08) when doped in CBP as a host. The possibility of energy transfer from CBP to compound 2 was evidenced from PL spectra of CBP and absorption spectra of compound 2. The emitters 3 & 4 as a single-emitting component in multilayer device was used to achieve “pure” white light (CIE: 0.34, 0.32) and electromer formation were also confirmed by fabricating single layer device. This white light was considered as a combination of a blue emission band from excimers and an orange emission band from electromers at a high voltage. Our further research will focus on the optimization of device structures to improve performances.

Acknowledgements

N. N thank DST–INSPIRE program for the financial assistant as a JRF (IF10495). R. R and N. N thank DST, India, for their financial support in the form of a research grant (Ref. No. SR/S1/PC–12/2011, dt. 20/09/2011). G. V thanks University Grants Commission (UGC), India for the financial support in the form of Science Meritorious Student Fellowship. P. V thanks Department of Science & Technology for Major Research Project (Ref. No: SR/S1/PC–52/2012). Authors also thank UGC/DST–FIST for UV–VIS and Fluorescence facilities in the School of Chemistry, Bharathidasan University. We are thankful to Prof. P. Ramamurthy, NCUPF, University of Madras, Chennai for providing TCSPC and Laser flash photolysis instrumental facilities.

Appendix A. Supplementary data

Supplementary data related to this article can be found at <http://dx.doi.org/10.1016/j.dyepig.2013.11.002>.

References

- [1] Tang CW, VanSlyke SA. *Appl Phys Lett* 1987;51:913–5.
- [2] Zhu Y, Tour JM. *Nat Photonics* 2012;6:72–3.
- [3] Kulkarni AP, Tonzola CJ, Babel A, Jenekhe SA. *Chem Mater* 2004;16:4556–73.
- [4] Li Z, Li ZR, Meng H. *Organic light-emitting materials and devices*. Taylor & Francis; 2010.
- [5] Farinola GM, Ragni R. *Chem Soc Rev* 2011;40:3467–82.
- [6] Chen C-H, Huang W-S, Lai M-Y, Tsao W-C, Lin JT, Wu Y-H, et al. *Adv Funct Mater* 2009;19:2661–70.
- [7] Tang S, Liu MR, Lu P, Xia H, Li M, Xie ZQ, et al. *Adv Funct Mater* 2007;17:2869–77.
- [8] Kwon JE, Park SY. *Adv Mater* 2011;23:3615–42.
- [9] Li JY, Liu D, Ma CW, Lengyel O, Lee CS, Tung CH, et al. *Adv Mater* 2004;16:1538–41.
- [10] Xu X, Yu G, Di Ca, Liu Y, Shao K, Yang L, et al. *Appl Phys Lett* 2006;89:123503-3.
- [11] Zhao Z, Xu B, Yang Z, Wang H, Wang X, Lu P, et al. *J Phys Chem C* 2008;112:8511–5.
- [12] Liu Y, Nishiura M, Wang Y, Hou Z. *J Am Chem Soc* 2006;128:5592–3.

- [13] Abbel R, Grenier C, Pouderoijen MJ, Stouwdam JW, Lacleère PELG, Sijbesma RP, et al. *J Am Chem Soc* 2008;131:833–43.
- [14] D'Andrade BW, Forrest SR. *Adv Mater* 2004;16:1585–95.
- [15] Lee Y-Z, Chen X, Chen M-C, Chen S-A, Hsu J-H, Fann W. *Appl Phys Lett* 2001;79:308–10.
- [16] Granlund T, Pettersson LAA, Anderson MR, Inganas O. *J Appl Phys* 1997;81:8097–104.
- [17] Berggren M, Gustafsson G, Inganas O, Andersson MR, Hjertberg T, Wennerstrom O. *J Appl Phys* 1994;76:7530–4.
- [18] Adhikari RM, Duan L, Hou L, Qiu Y, Neckers DC, Shah BK. *Chem Mater* 2009;21:4638–44.
- [19] Agrawal AK, Jenekhe SA. *Chem Mater* 1996;8:579–89.
- [20] Tao S, Li L, Yu J, Jiang Y, Zhou Y, Lee C-S, et al. *Chem Mater* 2009;21:1284–7.
- [21] Svensson M, Zhang F, Veenstra SC, Verhees WJH, Hummelen JC, Kroon JM, et al. *Adv Mater* 2003;15:988–91.
- [22] Wang Z, Lu P, Chen S, Gao Z, Shen F, Zhang W, et al. *J Mater Chem* 2011;21:5451–6.
- [23] Zhang Y, Lai S-L, Tong Q-X, Lo M-F, Ng T-W, Chan M-Y, et al. *Chem Mater* 2011;24:61–70.
- [24] Huang H, Yang X, Pan B, Wang L, Chen J, Ma D, et al. *J Mater Chem* 2012;22:13223–30.
- [25] Yang X, Zheng S, Bottger R, Chae HS, Tanaka T, Li S, et al. *J Phys Chem C* 2011;115:14347–52.
- [26] Park S, Kwon JE, Kim SH, Seo J, Chung K, Park S-Y, et al. *J Am Chem Soc* 2009;131:14043–9.
- [27] Morris JV, Mahaney MA, Huber JR. *J Phys Chem* 1976;80:969–74.
- [28] Frisch M, Trucks G, Schlegel HB, Scuseria G, Robb M, Cheeseman J, et al. Wallingford, CT: Inc.; 2009:270–271.
- [29] Becke AD. *J Chem Phys* 1993;98:5648–52.
- [30] Perdew JP. *Phys Rev B* 1986;33:8822–4.
- [31] Becke AD. *Phys Rev A* 1988;38:3098–100.
- [32] Lee C, Yang W, Parr RG. *Phys Rev B* 1988;37:785–9.
- [33] Foresman JB, Head-Gordon M, Pople JA, Frisch MJ. *J Phys Chem* 1992;96:135–49.
- [34] Runge E, Gross EKV. *Phys Rev Lett* 1984;52:997–1000.
- [35] Stratmann RE, Scuseria GE, Frisch MJ. *J Chem Phys* 1998;109:8218–24.
- [36] Bauernschmitt R, Ahlrichs R. *Chem Phys Lett* 1996;256:454–64.
- [37] Casida ME, Jamorski C, Casida KC, Salahub DR. *J Chem Phys* 1998;108:4439–49.
- [38] Perdew JP, Burke K, Ernzerhof M. *Phys Rev Lett* 1996;77:3865–8.
- [39] Adamo C, Barone V. *J Chem Phys* 1999;110:6158–70.
- [40] Miertuš S, Scrocco E, Tomasi J. *Chem Phys* 1981;55:117–29.
- [41] Yang Y, Zhao J-F, Liu R-R, Li J-W, Yi M-D, Xie G-H, et al. *Tetrahedron* 2013;69:6317–22.
- [42] Xie L-H, Hou X-Y, Hua Y-R, Huang Y-Q, Zhao B-M, Liu F, et al. *Org Lett* 2007;9:1619–22.
- [43] Velusamy M, Hsu Y-C, Lin JT, Chang C-W, Hsu C-P. *Chem Asian J* 2010;5:87–96.
- [44] Kumar D, Thomas KRJ. *J Photochem Photobiol A – Chem* 2011;218:162–73.
- [45] Joswick MD, Campbell IH, Barashkov NN, Ferraris JP. *J Appl Phys* 1996;80:2883–90.
- [46] Poriel C, Metivier R, Rault-Berthelot J, Thirion D, Barriere F, Jeannin O. *Chem Commun* 2011;47:11703–5.
- [47] Tenderholt AL. Stanford, CA, USA: Stanford University 2007.